technologies

MDPI

Review

Quantum Sensing of Noisy and Complex Systems under Dynamical Control

Gershon Kurizki [1,*], Gonzalo A. Alvarez [2] and Analia Zwick [2,3]

[1] Weizmann Institute of Science, Rehovot 76100, Israel
[2] Centro Atómico Bariloche, CNEA, CONICET, 8400 S. C. de Bariloche, Argentina; gonzalo.a.alvarez@gmail.com (G.A.A.); any.zwick@gmail.com (A.Z.)
[3] Instituto de Física Enrique Gaviola, CONICET and Facultad de Matemática, Astronomía y Física, Universidad Nacional de Córdoba, 5000 Córdoba, Argentina
* Correspondence: gershon.kurizki@weizmann.ac.il; Tel.: +972-8-934-2365

Academic Editor: Alexander V. Sergienko
Received: 31 July 2016; Accepted: 14 December 2016; Published: 24 December 2016

Abstract: We review our unified optimized approach to the dynamical control of quantum-probe interactions with noisy and complex systems viewed as thermal baths. We show that this control, in conjunction with tools of quantum estimation theory, may be used for inferring the spectral and spatial characteristics of such baths with high precision. This approach constitutes a new avenue in quantum sensing, dubbed quantum noise spectroscopy.

Keywords: quantum noise; quantum dynamical control; quantum estimation; quantum sensing

1. Introduction

Nanoscale sensing may be defined as the gathering of information concerning the structure, properties or dynamics of atomic, molecular, or condensed-matter systems by probes capable of nanometric resolution. Such probes are amenable to quantum-mechanical description even though their quantumness, i.e., quantum coherence or entanglement, may or may not play a role in the sensing process. If the goal is to acquire quantum information (QI), i.e., read out the state of the probed system, then measurements of quantum correlations within or among probes become indispensable [1]. We, however, focus here on the much more robust and readily obtainable classical information on the system by simple quantum probes: either single or correlated qubits that are engineered to possess advantageous properties for the sensing process in question: Thus, superconducting qubits are excellent detectors of microwave or far-infrared photons [2]; Rydberg-atom qubits are highly sensitive probes of dipolar forces; and nitrogen-vacancy centers (NVC) in diamond are the most sensitive magnetometers or electrometers to date [3–7]. We shall not be concerned with the probing of mechanical degrees of freedom (phonon modes) for which the most appropriate probes are harmonic oscillators, as in optomechanical setups [8]. The peculiarity of the approach we present here is that rather than try to maximize the signal-to-noise ratio (SNR) obtainable by the probe, we set out to analyze and extract information from the noise exerted by the system on the probe [9]. Namely, the spectrum of fluctuations may be a viable source of information concerning a noisy, complex system which we shall treat as a "bath", e.g., a large molecule, an aggregate of interacting spins, a liquid, or stray fields at diverse frequencies. This emerging area of research, nicknamed "noise spectroscopy" [9–13], requires a detailed consideration of the probing process, in which we schematically discern the following stages: change of the probe state under the influence of the noise and control; transfer and storage of this state or at least its partial information content to either a storage device or an information processor for processing or improving the sensing process; readout and analysis of the extracted information.

Each of these stages may greatly benefit from (at least partial) knowledge of the noise characteristics. On the assumption that the noise spectrum is stationary, we may undertake its complete mapping [10,11]. This, however, is a laborious and time-consuming undertaking. Instead, it may suffice to record only a few parameters of the noise that provide a distinct signature of the bath: the bath structure and the dynamics of the underlying processes (e.g., diffusion, collisions and thermal fluctuations [9,14–19]). We show here that such tasks may be accomplished with high fidelity or success probability by subjecting the probe to an appropriate dynamical control that may turn a sub-optimal into a fully optimal probing/sensing process. Similar considerations apply to the transfer, storage and readout of the probed noise characteristics.

Noise-spectrum information obtainable by quantum probing/sensing is particularly important not only for QI processing [10–12,20–22] and quantum metrology [23–27] but also for the design of quantum thermal (heat) machines [28–33] and, most intriguingly, for biomedical diagnostics based on NMR and MRI [11,14–19].

The conceptual unified framework for the treatment of the appropriate control and information extraction is provided by a method we dub bath-optimized task-oriented control (BOTOC) [34,35] which is expounded in Section 2 and compared to dynamical decoupling (DD) [36–42]. In Section 3 we show how noise spectra may be extracted using BOTOC by the qubit probe [10,11]. Section 4 is dedicated to optimized estimation of the noise parameters, with a focus on a qubit probe [9]. In Sections 5 and 6, we discuss the transfer of the noise information from the qubit probe to a storage qubit [34,35] or through a quantum channel [43], respectively, under control derived from BOTOC that optimizes the fidelity or duration of the transfer. We also discuss the benefit of BOTOC for extracting information of the quantum channel. In Section 7 we extend the discussion of BOTOC to multiqubit probing [44–49] of correlations in the noise (fluctuations) of composite systems treated as baths. Section 8 is dedicated to the conclusions, with more discussion of the comparison between BOTOC and DD, and an outlook that outlines open issues.

2. Bath-Optimized Task-Oriented Control (BOTOC)

Our general framework, dubbed BOTOC, allows for controlling the interaction of a quantum probe with its (usually multiple) baths, and is aimed at optimally executing a chosen operation, whether unitary or non-unitary. Examples are: state-transfer or storage with the highest fidelity possible, state purification, entanglement distribution, or energy transfer. To this end, we design the temporal control of the Hamiltonian that governs the system, subject to variational minimization or maximization (as the case may be) of a functional that quantifies the success probability of the operation. The control must be faster than the bath correlation (memory) time in order to counter or change bath-induced decoherence. For certain tasks, our control (BOTOC) may also *benefit from the probe-bath interactions* when the operation is non-unitary, e.g., state purification [34,35]. BOTOC is not limited to pulsed control, as opposed to DD [36–42], and thus may drastically reduce the energy and control errors if a smoothly varying field is employed instead of pulses [34,35]. These considerations remain true for our present purpose: the use of BOTOC as a tool of bath (quantum noise) diagnostics by quantum probes.

The bath response function is usually associated with a characteristic correlation or memory, τ, which separates the non-Markovian ($t \ll \tau$) and the Markovian ($t \gg \tau$) regimes, as in the case of an exponentially decaying bath-memory functional $\Phi(t) \propto e^{-\frac{t}{\tau}}$. Within the bath memory time, the bath modes oscillate in unison, and preserve the "memory" of their prior interaction with the system, whereas after the correlation time has passed, the modes lose their mutual coherence and "forget" their previous interactions [50–53].

The reason that the control of a quantum probe must be faster than the correlation (memory) time of the bath to which it couples is because it must compete with quasi-reversible/coherent dynamics induced by the bath. Such quasi-reversible dynamics is manifest by the quantum Zeno or anti-Zeno effects (QZE or AZE, respectively) [44–49,54–63]. The QZE and AZE correspond to the suppression and enhancement, respectively, of the bath effects via control. Dynamical control methods based on

the QZE are aimed at protecting the quantumness (coherence or entanglement) of the probe [45,63,64], but also at diagnosing the bath spectra [9,15,65] and transferring QI via noisy media [43,66–69]. By contrast, AZE-based control is useful for fast, versatile and robust cooling of thermalized quantum systems [51–53,70,71].

2.1. General Formulation of BOTOC

To lowest (i.e., second) order in the probe-bath interaction, $\hat{H}_{\rm I}$, the probability change of an Hermitian operator P over time t can be shown to obey

$$P = t^2 \langle [\hat{H}, \hat{P}] \hat{H} \rangle, \quad \hat{H} = \frac{1}{t} \int_0^t dt' \hat{H}_I(t') \tag{1}$$

where $\langle \cdot \rangle = {\rm Tr}[\hat{\rho}_{\rm tot}(0)(\cdot)]$ denotes averaging with respect to the initial state of the probe in the interaction picture [34,35].

We assume a d dimensional Hilbert-space of the probe, and expand the probe-bath interaction Hamiltonian of a controlled (driven or modulated probe) as a sum of products of probe and bath operators,

$$\hat{H}_I = \sum_{j=1}^{d^2-1} \hat{S}_j \otimes \hat{B}_j \tag{2}$$

In the interaction picture we may expand

$$\hat{S}_j(t) = \sum_k \varepsilon_{jk}(t) \hat{S}_k \tag{3}$$

in terms of (Hermitian, orthonormal) basis operators $\hat{S}_j$. This expansion defines a (real orthogonal) rotation matrix $\varepsilon(t)$ with elements in the probe's space

$$\varepsilon_{jk}(t) = \langle \hat{S}_j(t) \hat{S}_k \rangle, \tag{4}$$

These matrix elements are the correlation functions of the basis operators in the presence of a (driving) control.

The finite-time Fourier transform of this rotation matrix is denoted by the spectral functional

$$\varepsilon_t(\omega) = \frac{1}{\sqrt{2\pi}} \int_0^t {\rm d}t' \, {\rm e}^{{\rm i}\omega t'} \varepsilon(t'). \tag{5}$$

We next define a bath autocorrelation matrix $\Phi(t)$ with elements

$$\Phi_{jk}(t) = \langle \hat{B}_j(t) \hat{B}_k \rangle_{\rm B}, \tag{6}$$

and its (finite-time) Fourier transform, known as the bath spectral response (fluctuation spectrum)

$$G(\omega) = \int_{-\infty}^{\infty} {\rm d}t \, {\rm e}^{{\rm i}\omega t} \, \Phi(t). \tag{7}$$

The inverse of the bandwith over which $G(\omega)$ varies considerably, defines the bath correlation (memory) time τ.

Finally, we define a Hermitian matrix $\mathbf{\Gamma}$ with elements

$$\mathbf{\Gamma}_{kj} = \langle [\hat{S}_j, \hat{P}] \hat{S}_k \rangle. \tag{8}$$

Then we may cast the probability change of the operator in Equation (1) in the form of an overlap of two matrices

$$P = \iint_0^\infty \mathrm{d}t_1 \mathrm{d}t_2 \mathrm{Tr}[\varepsilon^T(t_1)\Phi(t_1 - t_2)\varepsilon(t_2)\,\mathbf{\Gamma}] \tag{9}$$

$$P = t\int_{-\infty}^{\infty} \mathrm{d}\omega\, \mathrm{Tr}[F_t(\omega)G(\omega)]. \tag{10}$$

In Equation (9) we have used the rotation matrix spectrum $\varepsilon_t(\omega)$ and the matrix $\mathbf{\Gamma}$ to define the probe spectral matrix, dubbed the "filter" functional

$$F_t(\omega) = \frac{1}{t}\varepsilon_t(\omega)\mathbf{\Gamma}{\varepsilon_t}^\dagger(\omega), \tag{11}$$

determined by the control field-intensity spectrum and its time duration t.

Equation (10) demonstrates that the change P over a given time t is determined by the spectral overlap between the controlled-probe and the bath dynamics [34,35,46–49]. The bath-spectral matrix $G(\omega)$ must be positive semi-definite for all ω.

In general, $F_t(\omega)$ is Hermitian but not necessarily positive semi-definite. This reflects the fact that the probability P can increase or decrease over t, according to the choice of $\mathbf{\Gamma}$, depending on whether our control is meant to maximize or minimize P [34,35].

This formulation may be used to optimize the success probability P of *any* operation performed on a quantum probe whose weak interaction with thermal baths is dynamically controlled [34,35]. It applies to any such control, be it coherent or projective (non-unitary), continuous or pulsed. Moreover, this optimization may be done under constraints on the total control energy E introduced by controlling the probe.

If P is the decoherence probability that should be minimized, this implies we must resort to the QZE-based control, namely, minimization of the integral product (overlap) of $G(\omega)$ and $F_t(\omega)$. The filter functional is the control handle on our ability to optimally execute the task in the presence of a given bath or several baths [34,46–49].

QZE-based control is required in operations related to QI storage and transmission [43,68], where bath effects are detrimental and must be suppressed. As shown here, it is likewise instrumental for *extracting information on the bath characteristics* [9,15]. Regardless of the chosen form of control, the controlled-probe dynamics must then be *Zeno-like*, namely, result in suppressed probe-bath interaction.

Alternatively, we may implement anti-Zeno (AZE) control, namely, *maximized overlap* of $G(\omega)$ and $F_t(\omega)$ (again, under control-energy constraints). AZE-control is instrumental for non-unitary operations that change the probe's entropy and benefit from efficient interaction with a bath for their execution [31,51–53,70]. If the underlying dynamics is anti-Zeno-like, probe-bath interaction will be enhanced and thereby facilitate these tasks.

Entanglement via the bath may require maximized bipartite coupling, but minimized single-partite coupling with the bath [72–74]. This requires an interplay of QZE and AZE that may depend on the quantum statistics of the bath [65].

2.2. Dynamical Control of Qubit Dephasing (Decoherence)

A simple application of the foregoing framework is the control of qubit probe decoherence, or proper dephasing, that causes random frequency fluctuation characterized by the correlation time, τ. The dephasing rate, if no control is applied, is:

$$R(t) = \int_0^t dt' \Phi(t'), \tag{12}$$

where $\Phi(t)$ is dephasing autocorrelation function.

At times much longer than the correlation time, the decoherence rate approaches its asymptotic value $R = \lim_{t\to\infty} R(t)$ that satisfies $R \ll \tau^{-1}$.

We assume that the control (driving) field has a Rabi frequency $V(t)$ with amplitude

$$V_0 \gg R. \tag{13}$$

This is in fact a specific example of Equations (9) and (10), that yields a dynamically modified decoherence rate according to the universal Kofman-Kurizki (KK) formula [44–48,50,55,56,60]

$$R(t) = 2\pi \int_{-\infty}^{\infty} d\omega F_t(\omega) G(\omega), \tag{14}$$

where the filter function $F_t(\omega)$ is given by Equations (5) and (11) with

$$\varepsilon(t) = e^{-i\int_0^t V(t')dt'} \tag{15}$$

and

$$G(\omega) = \frac{1}{\pi} \int_0^{\infty} \Phi(t) \cos \omega t dt. \tag{16}$$

It follows from Equation (16) that $G(\omega)$ is a symmetric function,

$$G(-\omega) = G(\omega). \tag{17}$$

The *proper dephasing* rate associated with an exponentially decaying correlation function

$$\Phi(t) = Ae^{-|t|/\tau} \tag{18}$$

is given by

$$R = A\tau. \tag{19}$$

In the presence of a *constant* V_0 (continuous wave (CW) $V(t) = V_0$) it turns into

$$R = \frac{A\tau}{V_0^2\tau^2 + 1}. \tag{20}$$

Hence, provided $V(t)$ is sufficiently strong, the dephasing rate R can be *reduced* by the factor $(V_0\tau)^2 \ll 1$. This means that strong Rabi splitting can shift the qubit probe away from the noise bandwidth, or average out the noise effects. Periodic π-pulses may similarly suppress dephasing, if their period satisfies $V_0 = \frac{\pi}{\tau}$.

2.3. Modulation Forms

Under a general modulation

$$\varepsilon(t) = \sum_k \varepsilon_k e^{-i\nu_k t} \tag{21}$$

with frequencies

$$|\nu_k - \nu_{k'}| \geq \Delta \qquad \forall k \neq k', \ \ \nu_k (k = 0, \pm 1, \ldots) \tag{22}$$

the long-time decoherence rate is (Figure 1d):

$$R = 2\pi \sum_k |\varepsilon_k|^2 G(\omega_a + \nu_k), \tag{23}$$

Let us apply to the qubit probe an impulsive periodic phase-modulation, $\varepsilon(t) = e^{i[t/\tau]\varphi}$, consisting of phase jumps φ with period τ. This modulation can be a periodic AC-Stark shift to control decay or

a periodic resonant field to control decoherence. The power spectrum (filter function) of this control consists of equidistant Fourier (harmonic) peaks with the following frequencies and weights:

$$\nu_k = \frac{2k\pi - \varphi}{\tau}, |\varepsilon_k|^2 = \frac{4\sin^2(\varphi/2)}{(2k\pi - \varphi)^2} \tag{24}$$

For *small phase shifts*, $\varphi \ll 1$, the main contribution is that of the $k = 0$ harmonic,

$$|\varepsilon_0|^2 \approx 1 - \frac{\varphi^2}{12}, \tag{25}$$

the higher harmonic weights scaling as (Figure 1b)

$$|\varepsilon_k|^2 \approx \frac{\varphi^2}{(2k\pi)^2} \ (k \neq 0), \tag{26}$$

As $|\varphi|$ increases, the difference between the $k = 0$ and $k = 1$ weights diminishes until the phase jumps by $\varphi = \pi$

$$|\varepsilon_0|^2 = |\varepsilon_1|^2 \approx \frac{4}{\pi^2}\,. \tag{27}$$

Then, the filter function $F_t(\omega)$ has *two main symmetrically shifted peaks* (Figure 1c) while higher harmonics $|\lambda_k|^2$ decrease with k as $(2k-1)^{-2}$. This modulation then coincides with dynamical decoupling (DD) pulses [36–42].

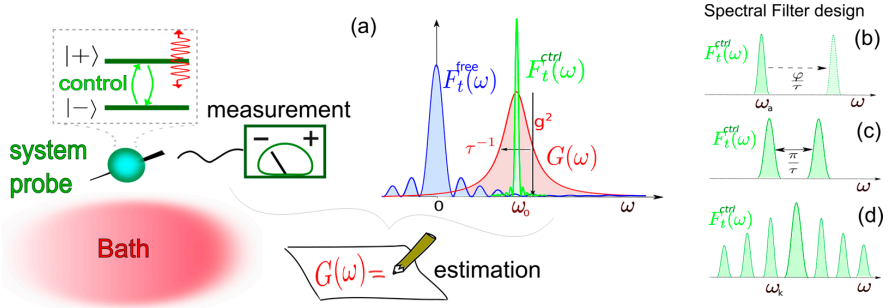

Figure 1. (**a**) Probing bath-induced decoherence by a system probe that is subject to control. Key bath parameters that define the bath spectrum $G(\omega)$, such as the correlation time τ and the bath-coupling coupling g, are estimated from measurements of the probe in the (anti-)symmetric superposition states. Spectral Filters $F_t(\omega)$ designed by: (**a**) Free evolution (blue sinc filter function), and Car-Purcell-Meiboom-Gill (CPMG) sequence control (green narrow band pass filter); (**b**) Modulation with small phase shifts, $\varphi \ll 1$; (**c**) π-pulses ($\varphi = \pi$) modulation; (**d**) Quasi-periodic modulation.

2.4. Optimal Decoherence Control of a Qubit

It is appropriate to compare the effect of dynamical decoupling (DD) [36–42] with that of BOTOC. DD does not change with the bath spectrum $G(\omega)$. With an increasing pulse rate, DD shifts the weight of the system spectrum $F_t(\omega)$ towards higher frequencies, until the overlap Equation (14) becomes sufficiently small. This DD procedure may, however, fail if the bath spectrum has a multipeak structure because then the overlap may increase rather than decrease with pulse rate whenever the vicinity of a peak is probed. By contrast, BOTOC is optimally tailored to any bath spectrum once it has been properly diagnosed by the probe.

Hence, DD sequences [36–42] may not be optimal for decoherence suppression, when they are insensitive to the bath spectral response (coupling spectrum). Instead, here we resort to the BOTOC approach outlined above [34,35], subject to minimal-energy constraints, so as to deduce

the *optimal, energy-constrained control* of a decohering qubit probe by modulation, for *any given bath-coupling spectrum*.

This is achieved by controlling the decoherence rate, $R(t)$, given a bath-coupling spectrum, $G(\omega)$, through the optimal phase modulation, $\varepsilon(t) = e^{i\phi(t)}$, according to the KK formula [44–46,50,55,56,60–62] of Equation (14), under the Euler–Lagrange optimization method subject to constraints such as the minimization of the total control energy,

$$\int_0^T dt|\dot{\phi}(t)|^2 = E \tag{28}$$

3. Control for Bath Diagnostics

Our main purpose here is to dynamically control qubit-bath coupling not as a means of fighting decoherence but as a tool of bath-spectrum (noise) diagnostics [9–11], and thereby study the dynamics of decoherence. This diagnostics is again based on Equation (14), the KK universal formula [44–46,50,55,56,60–62]. Even if the ultimate goal of any modulation scheme is to reduce, or, if possible, eliminate the decoherence, one must first know the probe-bath coupling spectra so as to obtain the optimal modulation using BOTOC [34,35]. This information is normally not available *a-priori* and thus one must use known, prescribed controls for revealing the unknown bath spectra that characterize the probe-bath coupling interaction, so then one can tailor optimal modulations for determined bath parameters.

The protocol consists in changing the filter function $F_t(\omega)$, e.g., by varying the control-field Rabi frequency, measuring the corresponding decoherence rate $R(t)$ and inferring $G(\omega)$ from the KK formula. The qubit probe is prepared at $t = 0$ in a superposition of its excited ($|\uparrow\rangle$) and ground ($|\downarrow\rangle$) energy states, $|\downarrow\rangle = \frac{1}{\sqrt{2}}(|\downarrow\rangle + |\uparrow\rangle)$, corresponding to a mean coherence that decays as

$$\langle\sigma_x(t)\rangle = e^{-R(t)t}\langle\sigma_x(0)\rangle, \tag{29}$$

$R(t)$ being the dynamically controlled decoherence rate.

The probability of the qubit to occupy the symmetric or antisymmetric superposition of the upper and lower states is then given by

$$p_{\pm}(t) = \frac{1 \pm e^{-R(t)t}}{2}. \tag{30}$$

One may infer $R(t)$ from these probabilities that are obtainable from measurements. We have experimentally demonstrated the reconstruction of the bath-coupling spectrum $G(\omega)$ by measurements performed on a trapped cold-atom ensemble [10], and on nuclear spin systems [11]. By monitoring the decoherence rate $R(t)$ using control fields that generate narrow band filters $F_t(\omega)$, like the ones described in Equation (24) and Figure 1a, we could scan the overlap integral in the KK formula of Equation (14) to infer the bath-coupling spectrum in the weak-coupling limit.

4. Maximized Information on Bath's Parameters by Dynamical Control

In order to further advance the noise spectroscopy approach and broaden its applicability, it is imperative to find the best general strategy for extracting environmental information from the qubit probe decoherence. Extracting the full noise spectrum is a very demanding process, and usually contains more information than required for diagnostic purposes. The strategy we adopt to improve the noise spectroscopy approach is to estimate key parameters that characterize the bath spectrum and make a faster and precise diagnostic. We aim at minimizing the error in estimating these bath key parameters x_B by N_m measurements performed on the qubit probe (Figure 1a), which obeys the bound

$$\xi(x_B, t) = \frac{\delta x_B}{x_B} \geq \frac{1}{x_B\sqrt{N_m F_Q(x_B, t)}}, \tag{31}$$

derived by resorting to quantum estimation tools [75].

Here, the dependence of the controlled decoherence rate $R(t) \equiv R(x_B, t)$ on $G(\omega) \equiv G(x_B, \omega)$ is used in the expression for the quantum Fisher Information (QFI) [9,13,75]

$$F_Q(x_B, t) = \frac{e^{-2R(x_B,t)\,t}}{1 - e^{-2R(x_B,t)\,t}} \left(\frac{\partial R(x_B, t) t}{\partial x_B} \right)^2. \tag{32}$$

The relative error $\xi(x_B, t)$, Equation (31), may be minimized either *per measurement* N_m or per *total interrogation time* $T = N_m t$ [9], both alternatives being of practical importance in experimental situations. Then, for the minimal relative error per measurement, the QFI has to be maximized:

$$F_Q(x_B, t_{opt}) = \max_t F_Q(x_B, t) \tag{33}$$

which amounts to measuring the qubit state at the optimal time and optimally controlling the qubit probe. For the minimal $\xi(x_B, t)$ per total interrogation time, the QFI *per unit of time* needs to be maximized:

$$\frac{F_Q(x_B, t_{opt})}{t_{opt}} = \max_t \frac{F_Q(x_B, t)}{t} \tag{34}$$

Typical environments of interest for sensing are those undergoing a diffusion process characterized by a generalized Ornstein-Uhlenbeck spectral density

$$G(x_B, \omega) = \frac{A_\alpha g^2 \tau}{(1 + \omega^\alpha \tau^\alpha)}, \tag{35}$$

with $\alpha \geq 2$ and the renormalization factor A_α.

We have shown that there is an *ultimate accuracy bound* for the estimation per measurement of the key parameters x_B, such as the probe-bath coupling strength g and the correlation time τ, that may be achieved *only* under adequate control of the probe [9]. This knowledge allows for the design of the appropriate dynamical control strategy for each key parameter. For example, the maximal accuracy on g is attained by stroboscopic measuring of the probe at the QZE regime [9], while τ is attained by a CPMG sequence control on the probe which generates a narrow spectral filter [9,13].

On other hand, if uncontrollable noise sources are also present, which are not of interest for the sensing process such as an intrinsic T_2 decoherence due to a white noise (Markovian) process or due to pulse imperfections, we have resorted to more elaborate controls to selectively address the targeted noise source and key parameters. We therefore nicknamed the method "selective dynamical recoupling" (SDR) [14,16]. We have already implemented SDR to selectively monitor diffusion processes characterized by Equation (35) with $\alpha = 2$ and $A_\alpha = \pi^{-1}$, so as to determine the probe-environment coupling strengths [18] and the environmental correlation time, as well as diffusion restriction lengths [16,17,19] in systems of biological and chemical interest.

5. Dynamical Control of Quantum Transfer as Means of Diagnosing a Bath in Hybrid Systems

Commonly, manipulations of QI can be schematically divided into three stages: "writing-in," "storage," and "reading-out" [20–22,76]. Realistically, some systems are better suited for writing-in or reading-out than for storage, and vice versa. This has prompted the suggestion of *hybrid*, composite quantum systems [2]: quantum operations are rapidly performed and efficiently written in a qubit susceptible to decoherence, e.g., a Josephson (superconducting) qubit; then the QI is transferred (directly or via a link) to a storage qubit resilient to decoherence (encoded in an ensemble of, e.g., ultracold atoms); then, on demand, transferred back and read-out from the same fragile qubit.

Our aim is to examine a strategy for accomplishing the transfer with the highest fidelity and (or) speed to store or extend the life of the sensing information for improving the resolution of the sensing process. We also discuss relevant effects for extracting information in the bath characteristics from this

transfer. This quantum (state)-transfer in hybrids will be affected from a noisy subspace that is fragile against decoherence to a quiet, robust subspace, by choosing an appropriate dynamical control [43] that optimizes this QI transfer.

Optimized Transfer from Noisy to Quiet Qubits

The transfer of a quantum state from a fragile (noisy) qubit probe to a robust (quiet) qubit may be used as a means of diagnosis, i.e., extracting information on the bath. Here we consider two resonant qubits at ω_0 with temporally controlled interaction characterized by $V(t)$, the interaction strength that is adjustable by an external laser field [68], and descripted by the Hamiltonian $\hat{H}_c = V(t)\hat{\sigma}_x^{noisy} \otimes \hat{\sigma}_x^{quiet}$ where $\hat{\sigma}_i$, $i = x, y, z$ are the Pauli matrices. We choose the system-bath interaction Hamiltonian to be

$$\hat{H}_I = \hat{\sigma}_z^{noisy} \otimes \hat{B}(t) \tag{36}$$

where $\hat{B}(t)$ is the bath operator $\hat{B}$ rotating with the free-bath $\hat{H}_B$. This model represents proper dephasing in the probe noisy-qubit due to the bath operator $\hat{B}$, whereas the target quiet qubit is robust against decoherence.

The accumulated phase

$$\phi(t) = \int_0^t V(t')dt' \tag{37}$$

is our control parameter. In the absence of decoherence, the state transfer from qubit 1 to qubit 2 can be completed if at the final time, T, the phase $\phi(T)$ satisfies $\phi(T) = \frac{\pi}{2}$. Then, any state of the (probe) noisy qubit is mapped onto that of quiet qubit, initially in the ground state,

$$(\gamma|\downarrow\rangle + \beta|\uparrow\rangle)|\downarrow\rangle \rightarrow |\downarrow\rangle(\gamma|\downarrow\rangle - i\beta|\uparrow\rangle), \tag{38}$$

for any normalized γ, β.

By contrast, under decoherence, since the source noisy qubit is affected by the bath, the longer the information stays there, the lower the fidelity of the transfer. On the other hand, if the transfer is very fast, it may result in population leakage from $|\downarrow\rangle^{noisy}$ ($|\downarrow\rangle^{quiet}$) into $|\uparrow\rangle^{noisy}$ ($|\uparrow\rangle^{quiet}$). Such leakage [77] signifies the violation of the rotating wave approximation (RWA) when the transfer rate is comparable to the level distance of the qubits, ω_0.

We dwell here on bath effects in the RWA so that there is no leakage due to RWA breakdown, i.e., the transfer time being much slower than ${\omega_0}^{-1}$.

The general expression derived from Equations (9) and (10) for the averaged transfer fidelity at T is then:

$$\overline{F}(T) = 1 - \int_{-\infty}^{\infty} G(\omega)F_T(\omega)d\omega \tag{39}$$

The energy constraint E, defined in Equation (28), determines the minimum possible transfer time $T_{min} = \frac{\pi^2}{4E}$.

Here we illustrate the transfer fidelity for a Lorentzian bath spectrum. Surprisingly, when the memory time τ of the bath is comparable to or larger than the characteristic transfer time $\tau \gtrsim T_{min}$, the best solution actually performs a full transfer, $\phi(t) = \frac{\pi}{2}$, well within the control time, but rather than stop at $\phi = \frac{\pi}{2}$, it *overshoots* the transfer so that $\phi(t) > \frac{\pi}{2}$, and then returns slowly to $\frac{\pi}{2}$. During this interval, the information partially returns from the target (storage) qubit to the source (noisy) qubit probe. Then, similarly to the echo method, the noise acts to correct itself so that the non-Markovian bath effect is undone. This requires transfer times *significantly* larger than the minimal transfer time T_{min}, up to $10T_{min}$ or more, in order to achieve fidelity increases (up to 50% in Figure 2).

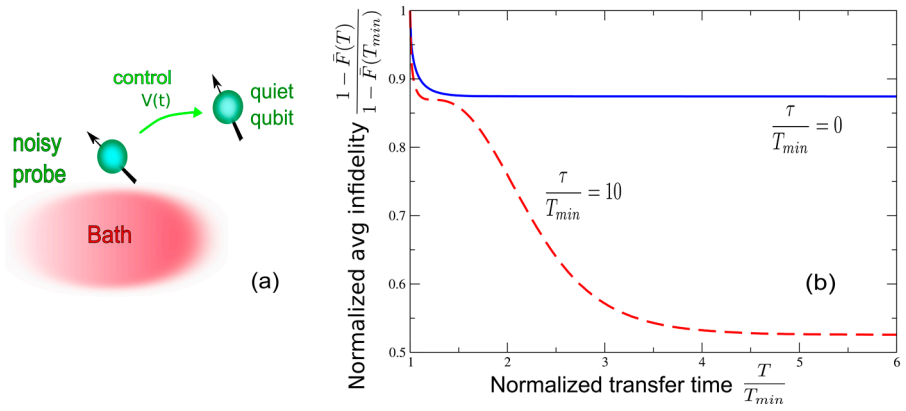

Figure 2. (**a**) Schematic view of the quantum state transfer (QST) process from a "noisy"qubit probe, due to the interaction with a bath, to the "quiet" qubit that may serve as robust storage of the information. Controlling the interaction $V(t)$ allows optimized QST; (**b**) Lowest achievable averaged infidelity as a function of the transfer time T normalized to the infidelity at the fastest transfer time T_{min} at a given transfer energy, plotted for (solid blue line) $\tau = 0$ (Markovian) and (dashed red line) non-Markovian baths $\tau/T_{min} = 10$. For non-Markovian baths ($\tau \gtrsim T_{min}$) two plateaux (regions of insensitivity to T) are found. The first plateau is independent of the memory time. The second plateau is lower for longer τ.

This method may be beneficial for the optimization of QI among different modules [2,66,67]: from superconducting qubit probes via a microwave resonator to ensembles of ultra-cold atoms or from NV-centers probe to nuclear spins [78].

To conclude, the state-transfer optimization within hybrid open systems, from a "noisy"qubit probe to its "quiet" counterpart, reveals the profound dependence of the transfer fidelity on the bath-memory time. Intriguingly, the fastest transfer is not optimal (for a given transfer energy). Hence, transfer fidelity maximization can disclose information on the bath non-Markovianity. Alternatively, one may use this method to significantly improve the storage and retrieval of QI in spectrally inhomogeneous spin ensembles [69] by preselecting an optimal portion of the ensemble via suitable control.

6. Dynamical Control of State Transfer via Noisy Quantum Channels and the Implications for Sensing Diagnostics

A similar approach may be used to exploit noisy quantum channels for state-transfer between the boundary (edge) qubits that are subject to temporal modulation and used for sensing. Alternatively, they can be exploited for diagnosis of the quantum channel. This modulation controls the coupling of the boundary system to the channels viewed as a fermionic bath. By means of this modulation one may design a spectral filter that suppresses the populations of noisy channel eigenmodes that impede successful transfer [43]. We show that under optimal modulation, the fidelity and the speed of transfer can be improved *by several orders of magnitude* at the fastest possible transfer for a given fidelity. This filtering effect may be used to infer the noisy channel characteristics from the transfer fidelity and speed.

6.1. Boundary Qubit Probes and State Transfer through a Quantum Channel

The Hamiltonian of a chain of $N + 2$ spin-1/2 parcticles with XX nearest-neighbor interactions has the form

$$\hat{H} = \hat{H}_{ch} + \hat{H}_{qp} \tag{40}$$

$$\hat{H}_{ch} = \sum_{i=1}^{N} V_i \sum_{\ell\in\{x,y\}} \hat{\sigma}_\ell^i \otimes \hat{\sigma}_\ell^{i+1},\ \hat{H}_{qp} = V(t) \sum_{\ell\in\{x,y\}} \left(\hat{\sigma}_\ell^{source} \otimes \hat{\sigma}_\ell^1 + \hat{\sigma}_\ell^N \otimes \hat{\sigma}_\ell^{target}\right) \tag{41}$$

Here $\hat{H}_{ch}$ and $\hat{H}_{qp}$ are the quantum channel and boundary-coupling probe Hamiltonians, respectively, and V_i are the spin-exchange couplings. To simplify the treatment, we diagonalize $\hat{H}_{ch}$ into the form $\hat{H}_{ch} = \sum_{k=1}^{N} \omega_k b_k^\dagger b_k$, where $b_k^\dagger$ populates a fermionic eigenstate $|\omega_k\rangle$ of energy ω_k. We may further simplify the model upon noticing that there is a single, zero-energy fermionic mode in the channel, $k = z = \frac{N+1}{2}$ [43] if we assume mirror (inversion) symmetry of the couplings $V_i = V_{N-i}$ for odd N. The boundary-qubit probes are resonantly coupled to ω_z with an effective, controlled interaction strength $\widetilde{V}(t)$. This resonant interaction is described by an effective Hamiltonian of the form

$$\hat{H}_S = s_+(t) b_z + h.c. \tag{42}$$

whereby the source and target (probe) mode operators are resonantly coupled to the zero-energy ($k = 0$) mode operator. These three fermionic modes constitute a "system" S that interacts with a "bath" B comprised of all other channel modes k (except for $k = 0$). On the basis of collective-mode operators associated with sums over the odd (even) bath-modes, the S-B interaction has the form

$$\hat{H}_{SB} = s_+(t) \sum_{k \in odd} \widetilde{V}_k b_k + s_-(t) \sum_{k \in even} \widetilde{V}_k b_k + h.c. \tag{43}$$

where $\widetilde{V}_k$ is the Fourier coefficient of the coupling to the kth mode. The dynamical control of this multipartite system then becomes similar to single-qubit level modulation [56,60–62] (Figure 3).

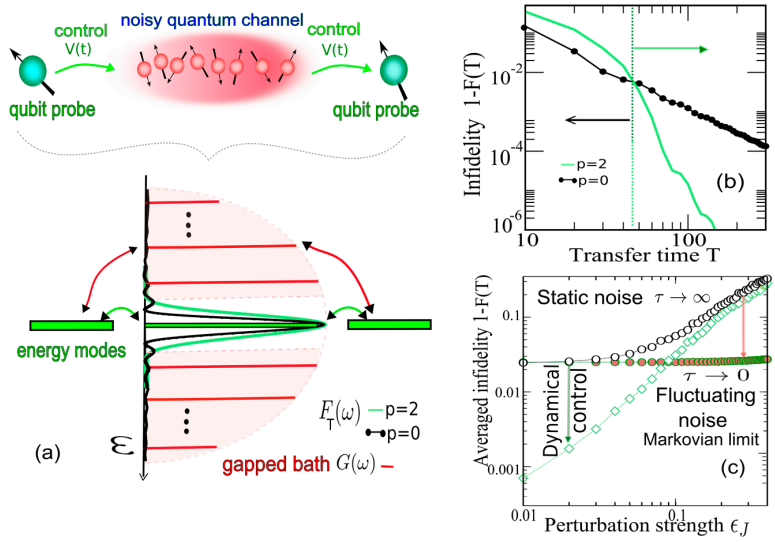

Figure 3. (**a**) Top: Controlled qubit probes coupled though a symmetric noisy quantum channel. In frequency space, the probes are resonantly coupled by a fermionic-mode of the channel whose energy is defined to be the energy origin (zero). These 3 degrees of freedom constitute the effective system (green rectangular bars); while the remaining channel modes are taken to be the bath (red lines) with a gapped spectrum $G_\pm(\omega)$. Under noise, the perturbed energies change/fluctuate bounded by the (colored gapped) Wigner-semicircle. In the gap, the optimal spectral-filters for the high fidelity state-transfer $F_{T,-}(\omega)$ correspond to dynamical boundary-control with $V(t)$: $p = 0$ (black dotted), $p = 2$ (green); (**b**) Transfer infidelity as a function of the transfer time T for the gapped Wigner-semicircle spectral bath: static control $p = 0$ (black dotted) and dynamic control $p = 2$ (green); (**c**) Averaged transfer infidelity $1 - \overline{F}(\boldsymbol{T})$ as a function of the perturbation strength ξ_V of the noisy channel. Dynamical $p = 2$ control (empty squares) strongly reduced the infidelity obtained under static control $p = 0$ (empty circles). A fluctuating noisy channel results in less damage than the static-noisy channel $\boldsymbol{\tau} \to \infty$, where its fidelity can even approach its unperturbed value in the Markovian limit $\tau \to 0$ ($p = 0$, green solid circles) . Here N = 29 channel-qubits and $V_i \equiv 1$.

To evaluate the transfer of any state of the source to the target qubit probes, we resort to a second-order solution of our non-Markovian master equation for the system density matrix [43] to obtain the state-transfer fidelity averaged over all possible input states. Similarly to Section 5, complete state transfer through the mediated mode, in the absence of a bath, occurs when the accumulated phase over time T, Equation (37), due to the modulation control $\widetilde{V}(t)$, satisfies $\phi(T) = \frac{\pi}{\sqrt{2}}$.

6.2. Optimized Filter Design for Channel Diagnostics

Modulation can control the transfer infidelity through the convoluted overlap of the bath and filter spectra governed by

$$\overline{F}(T) = 1 - \int_{-\infty}^{\infty} \sum G_{\pm}(\omega) F_{T,\pm}(\omega) d\omega \tag{44}$$

Here the $\pm$ indices are associated with the odd (even) parity modes that define the bath correlation functions $\phi_{\pm}(t) = \sum_{k \in odd(even)} V_k^2 e^{-i\omega_k t}$ of Equations (6) and (7) and the rotations due to the modulation control $\varepsilon_+(t) = V(t)\cos\left(\sqrt{2}\varphi(t)\right)$ and $\varepsilon_-(t) = V(t)$ of Equations (4), (5) and (11). The optimal modulation control minimizes the overlap integrals of $G_{\pm}(\omega)$ and $F_{T,\pm}(\omega)$ for a given transfer time T by the variational Euler-Lagrange (E-L) method under energy constraint E, Equation (29).

Since we assume the channel to be symmetric with respect to the source and target qubits and the number of eigenvalues to be odd, the central mode results in being invariant to noise. Then, by considering this central mode as part of the system, the bath spectrum $G_{\pm}(\omega)$ has a central gap (Figure 3a).

Therefore, to minimize the transfer infidelity, we need a narrow bandpass filter centered on the gap that minimizes the overlap between $G_{\pm}(\omega)$ and $F_{T,\pm}(\omega)$. Since $G_-(\omega)$ has a narrower gap than $G_+(\omega)$, optimal analytical solutions for the control of the boundary probes can be found by the BOTOC method to be [79]:

$$V(t) = V_0 \sin^p\left(\frac{\pi t}{T}\right),\ p = 0, 2,\ |V_0| \leq 1 \tag{45}$$

Here $p = 0$ signifies static control, while $p = 2$ stands for dynamical control during the time T and V_0 is T-dependent to satisfy $\phi(T) = \frac{\pi}{\sqrt{2}}$.

For $p = 0$, the minimal-energy constraint $E_{min} = \frac{\pi^2}{4T_{min}}$, yields the narrowest filter around the bath-gap, but has many wiggles on the tails (Figure 3a) which overlap with bath-modes damaging the transfer. By contrast, for the same transfer time T, the $p = 2$ bandpass is wider and requires higher control energy, $E_2 = \frac{3}{2}E_{min}$, but this filter is much lower (flat, without wiggles) at bath-frequencies.

Hence, the bandpass filter width and its overlap with bath-energies as a function of T can optimize the modulations $V(t)$. When there is a short T, $p = 0$ yields the highest fidelity, because the central peak of the filter is the narrowest. With a longer T, $p = 2$ will give rise to higher fidelity, because the filter tails crucially affect the overlap (Figure 3a,b), and the $p = 2$ filter can reduce the transfer fidelity by orders of magnitude in a noisy gapped bath.

The best tradeoff is obtainable for $p = 2$, as it yields a filter function without spectral tails. By chopping off the tails, one may reduce by several orders of magnitude the transfer infidelity (error) as well as the transfer time (Figure 3b). Thus, transfer guided by the optimized filter function can disclose the channel spectrum, particularly the effective gap width.

6.3. Diagnosing Noise Effects in Quantum Channels

Noise may affect the coupling strengths, causing: $V_i \to V_i + V_i\Delta_i(t)$, $i = 1 \ldots N$ where $\Delta_i(t)$ is a random variable in the interval $[-\xi_V, \xi_V]$, $\xi_V > 0$ being the noise strength. We consider *static (fluctuating) noise* when Δ_i is time-independent (dependent). These noises affect the bath-energy modes, while the central (zero) energy ω_z remains invariant, yet they are amenable to control:

(i) Dynamical boundary-control can make the channel most robust against static noise, because it filters out the bath-energies that damage the transfer. In Figure 3c $p = 2$ control is shown to be advantageous compared with the static control case $p = 0$, at the expense of increasing the transfer time by only a factor of 2.

(ii) Modulation is not helpful against Markovian noise. Remarkably, arbitrarily high fidelities can then be achieved by slowing down the transfer time, i.e., by decreasing V_0, because in a Markovian bath, the fast coupling fluctuations suppress disorder-localization effects that hamper the transfer fidelity.

(iii) For non-Markovian fluctuating noise $V_i + V_i\Delta_i(t)$, that randomly varies with correlation time τ (Figure 3b), in contrast to Markovian noise with $\tau \to 0$, optimized dynamical control can strongly reduce the infidelity that lies between the static and Markovian limits, provided the bath-spectrum is gapped.

Hence, BOTOC dynamical control of the tradeoff between transfer speed and fidelity of qubit-state transfer through a quantum channel can disclose the characteristics of noise on qubit-qubit couplings. The fidelity and/or the transfer speed can be enhanced by orders of magnitude by appropriate control, while their robustness against noise on the qubit-qubit couplings remains intact. Remarkably, static noise is more detrimental but also more controllable than fluctuating noise. Hence, control allows for a clear spectral signature of the noise.

The detailed spectral distribution of the $S-B$ coupling $G(\omega)$, is not required for BOTOC-based control design, only the spectral width and approximate mode spacing, which can be diagnosed by the methods of Section 4. Such channel noise diagnostics should suffice for designing the optimal tradeoff of the fidelity versus time transfer T by appropriate temporal modulation of the coupling.

7. Dynamical Control of Multipartite Probes for Bath Diagnostics

Decoherence control of a multiqubit probe coupled to a thermal bath, is much more challenging than that of a single-qubit probe, for a few reasons: (i) inter-qubit entanglement is more rapidly destroyed by the baths than single-qubit coherence [79]; (ii) cross-decoherence, namely mutual coupling of qubits via the baths, may complicate the control. We have nevertheless extended our decoherence control approach to multipartite scenarios [47,48,80].

The extension of our control formulation to decay and dephasing due to interaction with finite-temperature baths discloses additional information on the bath characteristics when one monitors the multipartite disentanglement in the time and spectral domains.

Namely, if one deals with a multipartite probe, one must apply multiple modulations that address the different qubits, on top of performing single-qubit modulations. This is essential in order to control the cross-coupling spectra of all possible qubit pairs [47,48], which are extremely important for reducing disentanglement and decoherence.

Our goal here is to exploit different modulations that effectively address different bath modes as a means of inferring the coupling strengths of these bath modes to different qubits comprising the probe. Subsequently, one may gather a wealth of information concerning the spatial and spectral structure of the bath.

7.1. Multipartite Decoherence Matrix

The decoherence rate (either due to decay or dephasing) of multiqubit probes weakly interacting with a thermal bath is an example of Equations (9) and (10), and similarly to Equation (14), it can be expressed in the spectral domain as a matrix with elements

$$R_{ij}(t) = 2\pi \int_{-\infty}^{\infty} d\omega G_{ij}(\omega) F_{t,ij}(\omega) \tag{46}$$

Here the diagonal elements of the decoherence matrix, R_{ii}, are the single-qubit probe decoherence rates. At long times and without control, the single-qubit probe modulation power spectrum, $F_{T,ii}(\omega)$ (see Equation (11), with $\mathbf{\Gamma} = \mathbf{I}$, where $\mathbf{I}$ is the identity operator), becomes a δ-function centered at the qubit energy separation, ω_a, resulting in a coupling between the qubit probe and a particular mode of the bath, with coupling strength $G(\omega_a)$, in accordance with Fermi's Golden Rule.

The off-diagonal element, R_{ij}, is comprised of the cross-relaxation rates of qubit i and j connected through the interaction with common bath modes, involving the overlap of the cross-coupling spectrum and the individual modulation spectra of the two qubits. Without modulations, the qubits comprising the probe that are coupled to *different* modes will not experience any cross-decoherence. Then, to induce cross-decoherence, the qubits should be properly controlled so as to couple them to the *common* modes with the same strength. Conversely, in order to eliminate cross-decoherence, one should locally modulate the qubits, at different rates, thereby coupling the two qubits to different modes.

What information can be inferred concerning the bath from such modulations? This issue will be discussed below.

7.2. Multiqubit Probe Modulations for Reconstructing Coupling Spectra

The multiqubit coupling spectra matrix, $G_{ij}(\omega)$, which is usually *unknown and is the objective of the sensing*, can be reconstructed through the knowledge of: (i) the decoherence matrix, $R_{ij}(\omega)$, which can be experimentally obtained via measurements of the decohering multiqubit probe; and (ii) the multiqubit modulation power-spectra matrix, $F_{T,ij}(\omega)$, which can be calculated for each specific *known* modulation.

Although our approach applies to any number of excitations, simpler solutions are obtainable for dynamically modified relaxation of singly excited multiqubit states.

Both the coupling spectrum matrix, $G_{ij}(\omega)$, and the dynamical modulation matrix, $F_{T,ij}(\omega)$ are then *complex* and not real, as in the single-qubit scenario. This occurs because, as opposed to the single-qubit probe scenario, the off-diagonal terms of the multiqubit modulation matrix are determined by the phases between modulations of the different qubits comprising the probe. The diagonal elements of the decoherence matrix are easily separable into real decay rates and imaginary Lamb shifts.

We first consider a probe comprised of N identical qubits, i.e., set $\omega_i \equiv \omega_a$, subject to impulsive-phase modulations (see below Equation (23)), requiring AC Stark shifts multiple of 2π at any chosen time $t = T$. Then, modulations only affect the decoherence matrix $R_{ij}(t)$, but do not change the relative phases of the entangled qubits when their states are probed or manipulated at $t = T$.

Without any modulations, decoherence in this multiqubit probe has no inherent symmetry, yet one can *symmetrize the decoherence* by appropriate controls. To this end different, local, phase-locked modulations may be applied to the individual qubits comprising the probe and may be chosen to cause *controlled interference* between the coupling of these qubits to the bath. The $F_{T,ij}(\omega)$ matrices can then satisfy $2N$ requirements at all times and be tailored to impose the symmetries detailed below. By contrast, a global modulation, i.e., when the same control is applied to all the qubit probes, characterized by $F_{T,ij}(\omega) = |\varepsilon_{T,i}(\omega)|^2$ is not guaranteed to satisfy $N \gg 1$ symmetrizing requirements at all times (Figure 4b).

The most convenient symmetry is that of *identical coupled particles* (ICP), which would emerge if all the controlled qubits comprising the probe could be subject to the following NxN matrix fully symmetrized for their decoherence

$$R_{ij}^{ICP}(t) = R(t) \quad \forall i, j. \tag{47}$$

The result would then be a $(N-1)$-dimensional single-excitation decoherence-free subspace (DFS). An initial multi-probe state in this DFS would be preserved for all times, i.e., it would lose neither its population nor its initial entanglement and the fidelity $F(t) = |\langle\psi(0)|\psi(t)\rangle|^2 = 1$.

This symmetry requires $N(N-1)/2$ conditions which cannot be ensured using N modulating fields. A more limited symmetry is that of *independent identical particles* (IIP), whereby the N different qubits comprising the probe experience the *same* single-qubit decoherence $R(t)$ but no

cross-decoherence (Figure 4a). This is achievable for $\varepsilon_{T,i}(\omega) \approx \varepsilon_{T,i}\delta(\omega - \Delta_i)$. The spectral shifts Δ_i can be different, so as to couple each qubit to a different frequency range of bath modes to ensure that their cross-coupling vanishes:

$$R_{ij}(t) = \varepsilon^*_{t,i}\varepsilon_{t,j} \int d\omega G(\omega)\delta(\omega - \Delta_i)\delta(\omega - \Delta_j) \to 0. \tag{48}$$

The N single-qubit decoherence rates can be made equal by an appropriate choice of N parameters $\{\Delta_i\}$:

$$R^{IIP}_{ij}(t) = |\varepsilon_{t,i}|^2 G_{ij}(\Delta_i) = \delta_{ij}R(t), \tag{49}$$

where $\delta_{i,j}$ is Kronecker's delta. Here, results conveniently express the fidelity of the initial multi-probe state as $F(t) = F_p(t)F_c(t)$, where $F_c(t)$ quantifies the correlation preservation, which is normalized with the population preservation $F_p(t)$ [47,48,80].

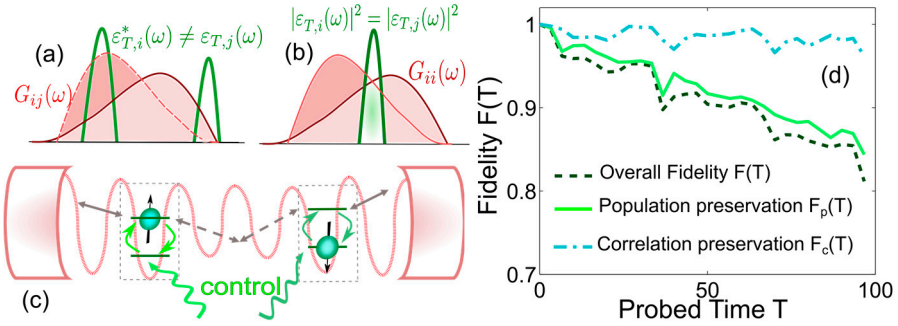

Figure 4. Overlap of coupling spectrum $G_{ij}(\omega)$, and modulation matrix elements $F_{T,ij}(\omega) = \frac{1}{t}\varepsilon^*_{T,i}(\omega)\varepsilon_{T,j}(\omega)$, resulting in modified decoherence matrix elements (overlap), for: (**a**) cross-decoherence elimination (IIP symmetry); and (**b**) global modulation (ICP symmetry); (**c**) Two qubits comprising a probe in a cavity. The qubits are coupled to the cavity modes (thin lines) and subject to local control fields (green lines); (**d**) Fidelity as a function of the probed time T of the IIP symmetry for the initial entangled two-qubit probe state $|\psi(0)\rangle = \frac{1}{\sqrt{2}}(|{\downarrow\uparrow}\rangle \pm |{\uparrow\downarrow}\rangle)$, coupled to a zero-temperature bath. The overall fidelity $F(T) = F_p(T)F_c(T)$ is in terms of the correlation preservation $F_c(T)$, and the population preservation $F_p(T)$. Two qubits comprising a probe in a cavity.

Then, by considering two qubit probes in a cavity as exemplified in Figure 4c, the IIP symmetry, Equation (49), results in the correlation fidelity $F_c(t) = 1$, yet this symmetry does not preclude and still permits population loss, so that the overall fidelity is then the same as the population fidelity, $F(t) = F_p(t) = e^{-Re\{R(t)\}}$. If the single-qubit decoherence rate $R(t)$ can be suppressed, i.e., if $G_{ii}(\omega_i + \Delta_i)$ is sufficiently small, this overall fidelity $F(t)$ will be kept close to 1 (Figure 4d).

Thus, the protocol outlined here is to use *different modulations* for each qubit, and measure the decoherence rate for each such modulation. The result is a vector of decoherence rates that depends on the modulation parameters. We can then find the coupling spectrum that best fits the calculated ($F_{T,ij}(\omega)$) and the measured ($R_{ij}(t)$) quantities.

A novel feature of a multiqubit probe under control is the *different modulation of each qubit*, $\varepsilon_j(t) \neq \varepsilon_j(t)$ (Figure 4a). The *phase difference* of the local modulations allows us to take advantage of interference between different decoherence channels, i.e., cross-decoherence. Different modulations may be designed to cause destructive interference and thus eliminate the cross-decoherence. Conversely, modulations of different qubits may give rise to a decoherence-free-subspace. Hence, control may bring out new distinctive characteristics of the bath cross-correlations between different bath modes or channels, and thus provide more bath-sensing information.

8. Conclusions

In this mini-review, we have surveyed our universal approach to the dynamical control of both single and multiple qubit probes subject to noise or decoherence by their environments viewed as baths for the purpose of diagnosing the noise spectra, thereby inferring the bath (environment) characteristics or extending the lifetime of the spin-probe state by transferring the information to a more isolated system for improving the resolution of the sensing process [78]. Such probes may operate at nanoscales, as magnetometers, thermometers, sensors for imaging or monitoring chemical and biological processes [9,14–19].

Our analysis of dynamically modified coupling between a qubit and a bath is based on the Kofman-Kurizki (KK) universal formula [44–46,50,55,56,60–62]. We have presented an approach (dubbed BOTOC—bath-optimized task-oriented control) towards finding the optimal time-dependence of the system Hamiltonian, such that a given observable attains a desired value [34,35,81]. This approach adapts the spectrum of the system modulation to the bath-coupling spectrum. In general, BOTOC requires information on the peak positions of the bath spectrum. Then, one may optimize the pulse timings and/or continuous control-parameters with respect to a given bath spectrum. Hence, BOTOC encompasses both pulsed and continuous modulation of the system Hamiltonian as limiting cases of control, and thus allows for vastly more freedom compared to control that is restricted to stroboscopic pulses as in some dynamical decoupling (DD) sequences [36–42]: BOTOC does not require rapidly changing control fields that approximate brief π-pulses. These features allow efficient optimization under a minimal energy constraint. On the other hand, a standard pulse sequence may be preferable experimentally.

Our main point here is that the same control can also be applied to map out the bath spectrum by measuring the decoherence rate for a narrow-band modulation centered at different frequencies [10,11]. Furthermore, this control may be optimized based on quantum estimation theory to infer the bath characteristics with the ultimate precision that this theory allows [9] and to selectively address key parameters by filtering out other sources of decoherence [14–19].

Our analysis of multiple, field-driven qubits that are coupled to partly correlated baths or undergo local random dephasing allows us to design both global and local control, based on different—but *synchronous*—local modulations of the different qubits [80]. The merits of local vs. global modulations are essentially twofold:

- Local modulation can effectively *decorrelate* the different dephasings of the multiple qubits, i.e., eliminate their cross-decoherence, resulting in their equal dephasing rates. For two qubits, the singlet and triplet Bell-states acquire the same dynamically modified decoherence rate.
- For different couplings to a bath, one can better preserve any initial state by local modulation, which can reduce the mixing with other states, than by global modulation. Local modulation which eliminates the cross-decoherence terms, increases the fidelity more than the global modulation alternative. For two qubits, local modulation better preserves an initial Bell-state, whether a singlet or a triplet, compared to global π-phase "parity kicks."

The conclusion from this analysis is that whenever qubits *collectively* couple to common bath modes (e.g., in ion traps [49] or cavities [47]) local modulations of individual qubits can eliminate cross-decoherence provided they are faster than the correlation (memory) time of the bath, but not necessarily than the much shorter multipartite coherence time. By observing the multipartite disentanglement, as a function of both local and global control, we may infer the cross-correlation between different bath modes (channels), both spatially and spectrally.

8.1. Comparison of Bath-Optimized Task-Oriented Control (BOTOC) to Dynamical Decoupling (DD)

Since dynamical decoupling (DD) techniques have also been recently employed in noise spectroscopy [82–89], in the wake of our pioneering work [10,11,13–19] it is appropriate to compare the two approaches.

Our BOTOC (universal-formula) approach is based on a general framework for *optimized* design of the modulation, which is desirable in order to accomplish a given task. This optimization consists in adjusting the "score" that quantifies the success of the task, such as the targeted fidelity, purity, entropy, or energy transfer by dynamical modification of the system-bath coupling spectrum on demand [26,27,29].

Several major differences make BOTOC advantageous compared to the DD approach:

(i) BOTOC relaxes the DD assumption that the control fields must be either very short or very strong. In our formalism, the control fields are considered *concurrently* with the coupling to the bath, hence allowing a much wider variety of pulse sequences, ranging from continuous modulation all the way to DD sequences.

(ii) Dynamical decoupling suggests using the same pulse sequence (be it periodic, optimized or concatenated), regardless of the shape of the bath spectrum. By contrast, BOTOC explicitly considers the bath spectrum and allows optimal tailoring of the modulation to a given bath spectrum. In many cases, the standard π-phase "bang-bang" is then found to be inadequate or non-optimal compared to dynamic control based on the optimization of the universal formula. Whereas our BOTOC approach reduces to the DD method in the particular case of proper dephasing or decay via coupling to *spectrally symmetric* (e.g., Lorentzian or Gaussian) noise baths with limited spectral width, phase modulation advocated for the suppression of coupling to baths with frequency cutoff or other non-monotonic spectra is, however, drastically different from the DD method which may fail for multipeak spectra.

(iii) Our BOTOC universal strategy has far broader applicability than DD: It can simultaneously control, unlike DD [10,11], both decay and decoherence (proper dephasing) by either pulsed or continuous wave (CW) modulation of the system-bath coupling governed by a *simple universal formula*. BOTOC has been generalized by us to finite temperatures and to qubits driven by an *arbitrary* time-dependent field, which may cause the failure of the rotating-wave approximation [11]. It has also been extended to the analysis of *multi-level systems*, where quantum interference between the levels may either inhibit or accelerate the decay [19].

(iv) Even if DD is adequate for independently decohering qubits, its extension to correlated multipartite systems is highly nontrivial. By contrast, BOTOC modulations with low energy *decorrelate* the different proper dephasings of the multiple two-level systems (TLS), resulting in equal dephasing rates for all states. For two TLS, we have shown that the singlet and triplet Bell-states acquire the same dynamically modified dephasing rate. This should be beneficial compared to standard DD based on global "bang-bang" (π-phase flips) if both the triplet and the singlet states are used (intermittently) for information transmission or storage.

8.2. Open Issues—Outlook

An open issue of the approach is the inclusion of higher orders in the system-bath coupling, which becomes important for strong or resonant system-bath coupling, so that the present perturbative approach cannot be applied. Concatenated DD [57] that treats increasingly higher order corrections of the noise, where each concatenation level of the control pulses reduces the previous level's induced errors, cannot be easily incorporated into our formalism since it goes beyond the second-order approximation used in our derivation of the universal formula.

Another standard assumption that may fail is that the initial state of the system and bath is factorized. Yet, if the system and the bath are in equilibrium, their state is entangled [55–57].

Hence, system-bath correlation is an important consideration that requires information on the corresponding parameters. It may be difficult to obtain such data with sufficient experimental precision. A way out is offered by a "closed" loop, based on actual measurements performed on the controlled system in real time rather than on prior knowledge of the bath properties. Such closed-loop control

would allow efficient optimization, but at the cost of losing any insight into the physical mechanisms behind the result obtained.

To conclude, the surveyed results show that dynamical control of decoherence is a promising avenue not only for combatting multipartite decoherence, since their rate is not required to become faster as the number of qubits grows, but also for inferring bath spectra. This new avenue may advance the quantum-sensing approach referred to as "quantum noise spectroscopy".

Acknowledgments: We acknowledge the ISF support under the Bikura (Prime) grant. Analia Zwick and Gonzalo A. Alvarez acknowledge the support from CONICET. Gonzalo A. Alvarez acknowledges the support of the European Commission under the Marie Curie Intra-European Fellowship for Career Development Grant No. PIEF-GA-2012-328605.

Author Contributions: All authors contributed to the research and to the writing of the article.

Conflicts of Interest: The authors declare no conflict of interest.

References

1. Modi, K.; Cable, H.; Williamson, M.; Vedral, V. Quantum correlations in mixed-state metrology. *Phys. Rev. X* **2011**, *1*, 021022. [CrossRef]
2. Kurizki, G.; Bertet, P.; Kubo, Y.; Molmer, K.; Petrosyan, D.; Rabl, P.; Schmiedmayer, J. Quantum technologies with hybrid systems. *Proc. Natl. Acad. Sci.* **2015**, *112*, 3866–3873. [CrossRef] [PubMed]
3. Balasubramanian, G.; Chan, I.Y.; Kolesov, R.; Al-Hmoud, M.; Tisler, J.; Shin, C.; Kim, C.; Wojcik, A.; Hemmer, P.R.; Krueger, A.; et al. Nanoscale imaging magnetometry with diamond spins under ambient conditions. *Nature* **2008**, *455*, 648–651. [CrossRef] [PubMed]
4. Steinert, S.; Ziem, F.; Hall, L.T.; Zappe, A.; Schweikert, M.; Götz, N.; Aird, A.; Balasubramanian, G.; Hollenberg, L.; Wrachtrup, J. Magnetic spin imaging under ambient conditions with sub-cellular resolution. *Nat. Commun.* **2013**, *4*, 1607. [CrossRef] [PubMed]
5. Kucsko, G.; Maurer, P.C.; Yao, N.Y.; Kubo, M.; Noh, H.J.; Lo, P.K.; Park, H.; Lukin, M.D. Nanometre-scale thermometry in a living cell. *Nature* **2013**, *500*, 54–58. [CrossRef] [PubMed]
6. Taylor, J.M.; Cappellaro, P.; Childress, L.; Jiang, L.; Budker, D.; Hemmer, P.R.; Yacoby, A.; Walsworth, R.; Lukin, M.D. High-sensitivity diamond magnetometer with nanoscale resolution. *Nat. Phys.* **2008**, *4*, 810–816. [CrossRef]
7. Meriles, C.A.; Jiang, L.; Goldstein, G.; Hodges, J.S.; Maze, J.; Lukin, M.D.; Cappellaro, P. Imaging mesoscopic nuclear spin noise with a diamond magnetometer. *J. Chem. Phys.* **2010**, *133*, 124105. [CrossRef] [PubMed]
8. Treutlein, P.; Genes, C.; Hammerer, K.; Poggio, M.; Rabl, P. Hybrid Mechanical Systems. In *Cavity Optomechanics*; Aspelmeyer, M., Kippenberg, T.J., Marquardt, F., Eds.; Quantum Science and Technology; Springer Berlin Heidelberg: Berlin, Germany, 2014; pp. 327–351.
9. Zwick, A.; Alvarez, G.A.; Kurizki, G. Maximizing information on the environment by dynamically controlled qubit probes. *Phys. Rev. Appl.* **2016**, *5*, 014007. [CrossRef]
10. Almog, I.; Sagi, Y.; Gordon, G.; Bensky, G.; Kurizki, G.; Davidson, N. Direct measurement of the system-environment coupling as a tool for understanding decoherence and dynamical decoupling. *J. Phys. B Mol. Opt. Phys.* **2011**, *44*, 154006. [CrossRef]
11. Álvarez, G.A.; Suter, D. Measuring the spectrum of colored noise by dynamical decoupling. *Phys. Rev. Lett.* **2011**, *107*, 230501. [CrossRef] [PubMed]
12. Bylander, J.; Gustavsson, S.; Yan, F.; Yoshihara, F.; Harrabi, K.; Fitch, G.; Cory, D.G.; Nakamura, Y.; Tsai, J.-S.; Oliver, W.D. Noise spectroscopy through dynamical decoupling with a superconducting flux qubit. *Nat. Phys.* **2011**, *7*, 565–570. [CrossRef]
13. Zwick, A.; Alvarez, G.A.; Kurizki, G. Criticality of environmental information obtainable by dynamically controlled quantum probes. *Phys. Rev. A* **2016**, *94*, 042122. [CrossRef]
14. Smith, P.E.S.; Bensky, G.; Álvarez, G.A.; Kurizki, G.; Frydman, L. Shift-driven modulations of spin-echo signals. *PNAS* **2012**, *109*, 5958–5961. [CrossRef] [PubMed]
15. Bretschneider, C.O.; Álvarez, G.A.; Kurizki, G.; Frydman, L. Controlling spin-spin network dynamics by repeated projective measurements. *Phys. Rev. Lett.* **2012**, *108*, 140403. [CrossRef] [PubMed]

16. Álvarez, G.A.; Shemesh, N.; Frydman, L. Coherent dynamical recoupling of diffusion-driven decoherence in magnetic resonance. *Phys. Rev. Lett.* **2013**, *111*, 080404. [CrossRef] [PubMed]
17. Shemesh, N.; Álvarez, G.A.; Frydman, L. Measuring small compartment dimensions by probing diffusion dynamics via Non-uniform Oscillating-Gradient Spin-Echo (NOGSE) NMR. *J. Magn. Reson.* **2013**, *237*, 49–62. [CrossRef] [PubMed]
18. Álvarez, G.A.; Shemesh, N.; Frydman, L. Diffusion-assisted selective dynamical recoupling: A new approach to measure background gradients in magnetic resonance. *J. Chem. Phys.* **2014**, *140*, 084205. [CrossRef] [PubMed]
19. Shemesh, N.; Álvarez, G.A.; Frydman, L. Size distribution imaging by Non-uniform Oscillating-Gradient Spin Echo (NOGSE) MRI. *PLoS ONE* **2015**, *10*, e0133201. [CrossRef] [PubMed]
20. Nielsen, M.A.; Chuang, I.L. *Quantum Computation and Quantum Information*; Cambridge University Press: Cambridge, UK, 2000.
21. Gisin, N.; Ribordy, G.; Tittel, W.; Zbinden, H. Quantum cryptography. *Rev. Mod. Phys.* **2002**, *74*, 145–195. [CrossRef]
22. Sergienko, A.V. *Quantum Communications and Cryptography*; CRC Press, Inc.: Boca Raton, FL, USA, 2005.
23. Giovannetti, V.; Lloyd, S.; Maccone, L. Advances in quantum metrology. *Nat. Photonics* **2011**, *5*, 222–229. [CrossRef]
24. Wolfgramm, F.; Vitelli, C.; Beduini, F.A.; Godbout, N.; Mitchell, M.W. Entanglement-enhanced probing of a delicate material system. *Nat. Photonics* **2013**, *7*, 28–32. [CrossRef]
25. Schmidt, P.O.; Rosenband, T.; Langer, C.; Itano, W.M.; Bergquist, J.C.; Wineland, D.J. Spectroscopy using quantum logic. *Science* **2005**, *309*, 749–752. [CrossRef] [PubMed]
26. Hempel, C.; Lanyon, B.P.; Jurcevic, P.; Gerritsma, R.; Blatt, R.; Roos, C.F. Entanglement-enhanced detection of single-photon scattering events. *Nat. Photonics* **2013**, *7*, 630–633. [CrossRef]
27. Ockeloen, C.F.; Schmied, R.; Riedel, M.F.; Treutlein, P. Quantum metrology with a scanning probe atom interferometer. *Phys. Rev. Lett.* **2013**, *111*, 143001. [CrossRef] [PubMed]
28. Gelbwaser-Klimovsky, D.; Alicki, R.; Kurizki, G. Minimal universal quantum heat machine. *Phys. Rev. E* **2013**, *87*, 012140. [CrossRef] [PubMed]
29. Gelbwaser-Klimovsky, D.; Alicki, R.; Kurizki, G. Work and energy gain of heat-pumped quantized amplifiers. *Europhys. Lett.* **2013**, *103*, 60005. [CrossRef]
30. Kolář, M.; Gelbwaser-Klimovsky, D.; Alicki, R.; Kurizki, G. Quantum Bath Refrigeration towards Absolute Zero: Challenging the Unattainability Principle. *Phys. Rev. Lett.* **2012**, *109*, 090601. [CrossRef] [PubMed]
31. Gelbwaser-Klimovsky, D.; Erez, N.; Alicki, R.; Kurizki, G. Work extraction via quantum nondemolition measurements of qubits in cavities: Non-Markovian effects. *Phys. Rev. A* **2013**, *88*, 022112. [CrossRef]
32. Alicki, R.; Gelbwaser-Klimovsky, D.; Kurizki, G. Periodically driven quantum open systems: Tutorial. *arXiv* **2012**, arXiv:1205.4552.
33. Gelbwaser-Klimovsky, D.; Kurizki, G. Work extraction from heat-powered quantized optomechanical setups. *Sci. Rep.* **2015**, *5*, 7809. [CrossRef] [PubMed]
34. Clausen, J.; Bensky, G.; Kurizki, G. Bath-optimized minimal-energy protection of quantum operations from decoherence. *Phys. Rev. Lett.* **2010**, *104*, 040401. [CrossRef] [PubMed]
35. Clausen, J.; Bensky, G.; Kurizki, G. Task-optimized control of open quantum systems. *Phys. Rev. A* **2012**, *85*, 052105. [CrossRef]
36. Viola, L.; Lloyd, S. Dynamical suppression of decoherence in two-state quantum systems. *Phys. Rev. A* **1998**, *58*, 2733–2744. [CrossRef]
37. Agarwal, G.S.; Scully, M.O.; Walther, H. Accelerating decay by multiple 2 pi pulses. *Phys. Rev. A* **2001**, *63*, 044101. [CrossRef]
38. Agarwal, G.S. Control of decoherence and relaxation by frequency modulation of a heat bath. *Phys. Rev. A* **2000**, *61*, 013809. [CrossRef]
39. Shiokawa, K.; Lidar, D.A. Dynamical decoupling using slow pulses: Efficient suppression of 1/f noise. *Phys. Rev. A* **2004**, *69*, 030302. [CrossRef]
40. Vitali, D.; Tombesi, P. Heating and decoherence suppression using decoupling techniques. *Phys. Rev. A* **2001**, *65*, 012305. [CrossRef]
41. Viola, L.; Knill, E. Robust dynamical decoupling of quantum systems with bounded controls. *Phys. Rev. Lett.* **2003**, *90*, 037901. [CrossRef] [PubMed]

42. Khodjasteh, K.; Lidar, D.A. Fault-tolerant quantum dynamical decoupling. *Phys. Rev. Lett.* **2005**, *95*, 180501. [CrossRef] [PubMed]
43. Zwick, A.; Álvarez, G.A.; Bensky, G.; Kurizki, G. Optimized dynamical control of state transfer through noisy spin chains. *New J. Phys.* **2014**, *16*, 065021. [CrossRef]
44. Gordon, G.; Kurizki, G.; Kofman, A.G. Universal dynamical control of local decoherence for multipartite and multilevel systems. *Opt. Comm.* **2006**, *264*, 398. [CrossRef]
45. Barone, A.; Kurizki, G.; Kofman, A.G. Dynamical control of macroscopic quantum tunneling. *Phys. Rev. Lett.* **2004**, *92*, 200403. [CrossRef] [PubMed]
46. Gordon, G.; Kurizki, G.; Kofman, A.G. Universal dynamical control of decay and decoherence in multilevel systems. *J. Opt. B* **2005**, *7*, 283. [CrossRef]
47. Gordon, G.; Kurizki, G. Preventing multipartite disentanglement by local modulations. *Phys. Rev. Lett.* **2006**, *97*, 110503. [CrossRef] [PubMed]
48. Gordon, G.; Erez, N.; Kurizki, G. Universal dynamical decoherence control of noisy single- and multi-qubit systems. *J. Phys. B Mol. Opt. Phys.* **2007**, *40*, S75–S93. [CrossRef]
49. Gordon, G.; Kurizki, G. Universal dephasing control during quantum computation. *Phys. Rev. A* **2007**, *76*, 042310. [CrossRef]
50. Kofman, A.G.; Kurizki, G. Theory of dynamical control of qubit decay and decoherence. *IEEE Trans. Nanotechnol.* **2005**, *4*, 116. [CrossRef]
51. Erez, N.; Gordon, G.; Nest, M.; Kurizki, G. Thermodynamic control by frequent quantum measurements. *Nature* **2008**, *452*, 724. [CrossRef] [PubMed]
52. Gordon, G.; Bhaktavatsala Rao, D.D.; Kurizki, G. Equilibration by quantum observation. *New J. Phys.* **2010**, *12*, 053033. [CrossRef]
53. Gordon, G.; Bensky, G.; Gelbwaser-Klimovsky, D.; Rao, D.; Erez, N.; Kurizki, G. Cooling down quantum bits on ultrashort time scales. *New J. Phys.* **2009**, *11*, 123025. [CrossRef]
54. Misra, B.; Sudarshan, E.C.G. Zeno's paradox in quantum theory. *J. Math. Phys.* **1977**, *18*, 756–763. [CrossRef]
55. Kofman, A.G.; Kurizki, G. Acceleration of quantum decay processes by frequent observations. *Nat. Lond.* **2000**, *405*, 546–550.
56. Kofman, A.G.; Kurizki, G. Universal dynamical control of quantum mechanical decay: Modulation of the coupling to the continuum. *Phys. Rev. Lett.* **2001**, *87*, 270405. [CrossRef] [PubMed]
57. Facchi, P.; Nakazato, H.; Pascazio, S. From the quantum Zeno to the inverse quantum Zeno effect. *Phys. Rev. Lett.* **2001**, *86*, 2699. [CrossRef] [PubMed]
58. Lane, A.M. Decay at early times—Larger or smaller than the Golden Rule. *Phys. Lett. A* **1983**, *99*, 359–360. [CrossRef]
59. Fischer, M.C.; Gutierrez-Medina, B.; Raizen, M.G. Observation of the quantum Zeno and anti-Zeno effects in an unstable system. *Phys. Rev. Lett.* **2001**, *87*, 040402. [CrossRef] [PubMed]
60. Kofman, A.G.; Kurizki, G. Unified theory of dynamically suppressed qubit decoherence in thermal baths. *Phys. Rev. Lett.* **2004**, *93*, 130406. [CrossRef] [PubMed]
61. Kofman, A.G.; Kurizki, G.; Opatrný, T. Zeno and anti-Zeno effects for photon polarization dephasing. *Phys. Rev. A* **2001**, *63*, 042108. [CrossRef]
62. Kofman, A.G.; Kurizki, G. Quantum Zeno effect on atomic excitation decay in resonators. *Phys. Rev. A* **1996**, *54*, R3750–R3753. [CrossRef] [PubMed]
63. Facchi, P.; Pascazio, S. Quantum Zeno subspaces. *Phys. Rev. Lett.* **2002**, *89*, 080401. [CrossRef] [PubMed]
64. Brion, E.; Akulin, V.M.; Comparat, D.; Dumer, I.; Harel, G.; Kèbaili, N.; Kurizki, G.; Mazets, I.; Pillet, P. Coherence protection by the quantum Zeno effect and nonholonomic control in a Rydberg rubidium isotope. *Phys. Rev. A* **2005**, *71*, 052311. [CrossRef]
65. Bhaktavatsala Rao, D.D.; Kurizki, G. From Zeno to anti-Zeno regime: Decoherence-control dependence on the quantum statistics of the bath. *Phys. Rev. A* **2011**, *83*, 032105. [CrossRef]
66. Petrosyan, D.; Bensky, G.; Kurizki, G.; Mazets, I.; Majer, J.; Schmiedmayer, J. Reversible state transfer between superconducting qubits and atomic ensembles. *Phys. Rev. A* **2009**, *79*, 040304. [CrossRef]
67. Bensky, G.; Amsüss, R.; Majer, J.; Petrosyan, D.; Schmiedmayer, J.; Kurizki, G. Controlling quantum information processing in hybrid systems on chips. *Quant. Inf. Proc.* **2011**, *10*, 1037–1060. [CrossRef]
68. Escher, B.M.; Bensky, G.; Clausen, J.; Kurizki, G. Optimized control of quantum state transfer from noisy to quiet qubits. *J. Phys. B Mol. Opt. Phys.* **2011**, *44*, 154015. [CrossRef]

69. Bensky, G.; Petrosyan, D.; Majer, J.; Schmiedmayer, J.; Kurizki, G. Optimizing inhomogeneous spin ensembles for quantum memory. *Phys. Rev. A* **2012**, *86*, 012310. [CrossRef]
70. Álvarez, G.A.; Rao, D.D.B.; Frydman, L.; Kurizki, G. Zeno and anti-Zeno polarization control of spin ensembles by induced dephasing. *Phys. Rev. Lett.* **2010**, *105*, 160401. [CrossRef] [PubMed]
71. Álvarez, G.A.; Bretschneider, C.O.; Fischer, R.; London, P.; Kanda, H.; Onoda, S.; Isoya, J.; Gershoni, D.; Frydman, L. Local and bulk 13C hyperpolarization in nitrogen-vacancy-centred diamonds at variable fields and orientations. *Nat. Commun.* **2015**, *6*, 8456. [CrossRef] [PubMed]
72. Kurizki, G.; Kofman, A.G.; Yudson, V. Resonant photon exchange by atom pairs in high-Q cavities. *Phys. Rev. A* **1996**, *53*, R35. [CrossRef] [PubMed]
73. Bhaktavatsala Rao, D.D.; Bar-Gill, N.; Kurizki, G. Generation of macroscopic superpositions of quantum states by linear coupling to a bath. *Phys. Rev. Lett.* **2011**, *106*, 010404. [CrossRef] [PubMed]
74. Bar-Gill, N.; Rao, D.D.B.; Kurizki, G. Creating nonclassical states of Bose-Einstein condensates by dephasing collisions. *Phys. Rev. Lett.* **2011**, *107*, 010404. [CrossRef] [PubMed]
75. Braunstein, S.; Caves, C. Statistical distance and the geometry of quantum states. *Phys. Rev. Lett.* **1994**, *72*, 3439–3443. [CrossRef] [PubMed]
76. Scully, M.O.; Zubairy, M.S. *Quantum Optics*; Cambridge University Press: Cambridge, UK, 1997.
77. Wu, L.-A.; Kurizki, G.; Brumer, P. Master equation and control of an open quantum system with leakage. *Phys. Rev. Lett.* **2009**, *102*, 080405. [CrossRef] [PubMed]
78. Laraoui, A.; Dolde, F.; Burk, C.; Reinhard, F.; Wrachtrup, J.; Meriles, C.A. High-resolution correlation spectroscopy of 13C spins near a nitrogen-vacancy centre in diamond. *Nat. Commun.* **2013**, *4*, 1651. [CrossRef] [PubMed]
79. Almeida, M.P.; de Melo, F.; Hor-Meyll, M.; Salles, A.; Walborn, S.P.; Ribeiro, P.H.S.; Davidovich, L. Environment-induced sudden death of entanglement. *Science* **2007**, *316*, 579. [CrossRef] [PubMed]
80. Gordon, G.; Kurizki, G. Scalability of decoherence control in entangled systems. *Phys. Rev. A* **2011**, *83*, 032321. [CrossRef]
81. Gordon, G.; Kurizki, G.; Lidar, D.A. Optimal dynamical decoherence control of a qubit. *Phys. Rev. Lett.* **2008**, *101*, 010403. [CrossRef] [PubMed]
82. Norris, L.M.; Paz-Silva, G.A.; Viola, L. Qubit noise spectroscopy for non-Gaussian dephasing environments. *Phys. Rev. Lett.* **2016**, *116*, 150503. [CrossRef] [PubMed]
83. Paz-Silva, G.A.; Viola, L. General transfer-function approach to noise filtering in open-loop quantum control. *Phys. Rev. Lett.* **2014**, *113*, 250501. [CrossRef] [PubMed]
84. Lang, J.E.; Liu, R.B.; Monteiro, T.S. Dynamical-decoupling-based quantum sensing: Floquet spectroscopy. *Phys. Rev. X* **2015**, *5*, 041016. [CrossRef]
85. Zhao, N.; Wrachtrup, J.; Liu, R.-B. Dynamical decoupling design for identifying weakly coupled nuclear spins in a bath. *Phys. Rev. A* **2014**, *90*, 032319. [CrossRef]
86. Ball, H.; Biercuk, M.J. Walsh-synthesized noise filters for quantum logic. *EPJ Quantum Technol.* **2015**, *2*, 11. [CrossRef]
87. Yan, F.; Gustavsson, S.; Bylander, J.; Jin, X.; Yoshihara, F.; Cory, D.G.; Nakamura, Y.; Orlando, T.P.; Oliver, W.D. Rotating-frame relaxation as a noise spectrum analyser of a superconducting qubit undergoing driven evolution. *Nat. Commun.* **2013**, *4*, 2337. [CrossRef] [PubMed]
88. Loretz, M.; Rosskopf, T.; Degen, C.L. Radio-frequency magnetometry using a single electron spin. *Phys. Rev. Lett.* **2013**, *110*, 017602. [CrossRef] [PubMed]
89. Yoshihara, F.; Nakamura, Y.; Yan, F.; Gustavsson, S.; Bylander, J.; Oliver, W.D.; Tsai, J.-S. Flux qubit noise spectroscopy using Rabi oscillations under strong driving conditions. *Phys. Rev. B* **2014**, *89*, 020503. [CrossRef]